JACS Au
AN OPEN ACCESS JOURNAL OF THE AMERICAN CHEMICAL SOCIETY

pubs.acs.org/jacsau
Article

Trapped in Cells: A Selective Accumulation Approach for Type-I Photodynamic Ablation of Cancer Stem−like Cells

Ji Hyeon Kim,[‖] Jieun Lee,[‖] Kyung-Woo Lee,[‖] Hao Xiong, Mingle Li,* and Jong Seung Kim*

Cite This: *JACS Au* 2024, 4, 3657−3667

Read Online

ACCESS | Metrics & More | Article Recommendations | Supporting Information

ABSTRACT: Aldehyde dehydrogenase (ALDH) is an enzyme responsible for converting aldehyde functional groups into carboxylate metabolites. Elevated ALDH activity is a characteristic feature of cancer stem-like cells (CSCs). As a novel approach to target the CSC trait of overexpressing ALDH, we aimed to utilize ALDH activity for the selective accumulation of a photosensitizer in ALDH^{High} CSCs. A novel ALDH substrate photosensitizer, **SCHO**, with thionylated coumarin and *N*-ethyl-4-(aminomethyl)-benzaldehyde was developed to achieve this goal. Our study demonstrated the efficient metabolism of the aldehyde unit of **SCHO** into carboxylate, leading to its accumulation in ALDH^{High} MDA-MB-231 cells. Importantly, we established the selectivity of **SCHO** as an ALDH^{High} cell photosensitizer as it is not a substrate for ABC transporters. **SCHO**-based photodynamic therapy triggers apoptosis and pyroptosis in MDA-MB-231 cells and further reduces the characteristics of CSCs. Our study presents a novel strategy to target CSCs by exploiting their cellular metabolism to enhance photosensitizer accumulation, highlighting the potential of photodynamic therapy as a powerful tool for eliminating ALDH^{High} CSCs.

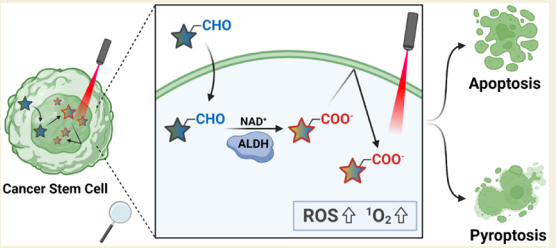

KEYWORDS: *aldehyde dehydrogenase, cancer stem cells, photosensitizer, thionylation, pyroptosis*

INTRODUCTION

Cancer stem cells (CSCs), also referred to as tumor-initiating cells (TICs), are a unique subset of cancer cells that can self-renew, differentiate, and proliferate indefinitely.[1−3] These cells are capable of evading conventional antineoplastic modalities, such as chemotherapy and radiotherapy, which can result in tumor recurrence or metastasis post-treatment.[4,5] As a result, concerted efforts are being devoted to developing innovative strategies aimed at selectively eradicating CSCs embedded within the neoplastic milieu.[6] However, despite the emergence of diverse approaches, ranging from the mitigation of mitochondrial H^+ leaks to the design of artificial ionophores (Figure 1A),[7−10] there is still a lack of clinically approved CSC-specific therapies.[11] In light of this challenge, researchers have been exploring safer and more effective therapeutic alternatives with unique mechanisms of action (MoA).[7,12−14] Here, we report an intriguing finding that involves leveraging the CSC metabolite, i.e., aldehyde dehydrogenase (ALDH) enzyme, to "trap" therapeutic drugs, offering a promising avenue for selectively eliminating CSCs (Figure 1B). We developed a first-generation ALDH-mediated activatable type-I photosensitizer named **SCHO** (Figure 1B). **SCHO** demonstrates a potential for triggering photodynamic CSC ablation through an MoA rooted in cell pyroptosis, as demonstrated in previous studies using two-dimensional culture cell models.

Photodynamic therapy (PDT) is a photon-controlled therapeutic modality that has garnered significant attention in cancer treatment, with a growing emphasis on carefully designing photosensitizers (PSs) to optimize therapeutic outcomes.[15,16] Although PDT offers the advantage of minimal invasiveness by applying light to the tumor region, it is still essential to selectively deliver PS to the tumor region to improve the efficacy. In recent years, numerous tumor-targeting strategies have been reported, such as antibody conjugation,[17] cell membrane receptor recognition,[18,19] and nanomedicine.[20] However, PDTs targeting CSCs are relatively rare, and methods for selectively accumulating PSs within CSCs have not been properly elucidated.

ALDH is an NAD(P)$^+$-dependent enzyme involved in alcohol metabolism, converting aldehydes into nonreactive acids. It processes aldehyde byproducts from amino acids, fats, and exogenous sources.[21] The resulting carboxylate metabolites are prone to be difficult to diffuse out of cells; therefore, they remain "trapped in cells.[22,23] Moreover, ALDH has been identified as a potential universal marker for CSCs and plays a crucial role in CSC maintenance and differentiation.[24] Elevated levels of ALDH1 in triple-negative breast cancer (TNBC) correlate with a poorer prognosis and are associated with a lower overall survival rate.[25,26] Hence, developing an ALDH-

Received: July 16, 2024
Revised: August 15, 2024
Accepted: August 16, 2024
Published: August 26, 2024

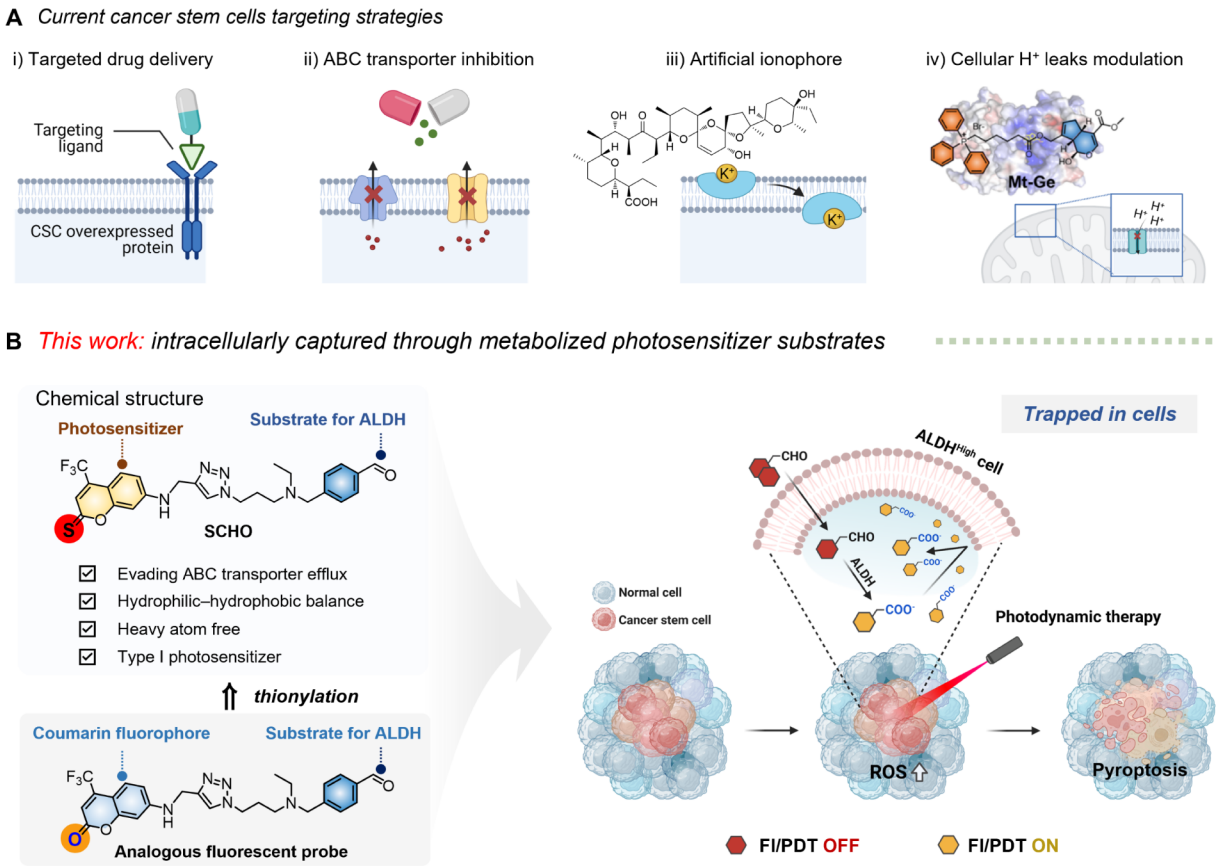

Figure 1. (A) Reported approaches for cancer stem cell–targeting modalities. (B) Chemical structure and properties of type-I PS **SCHO**, along with a schematic illustration of **SCHO** trapped in ALDH^{High} cancer stem–like cells.

specific PS holds promise for selective PS accumulation and phototherapy targeting of CSCs. However, several factors must be considered. The PS structure needs to strike a hydrophilic–hydrophobic balance, enabling easy cell membrane penetration and subsequent oxidation by the ALDH enzyme into carboxylate forms. Additionally, the PS should be resistant to drug efflux pumps, such as CSC-overexpressed ABC transporters, given the correlation with ALDH overexpression.[27] Last, dark toxicity should be minimized to leverage PDT's controllability spatiotemporally through light irradiation at the tumor site.

Considering these factors, we developed **SCHO**, a CSC-selective type I PS harboring ALDH activity. Our hypothesis suggested that *N*-ethyl-4-aminomethyl benzaldehyde would act as an ALDH recognition moiety.[28] We confirmed the oxidation of the aldehyde group to a carboxylate in the presence of ALDH enzymes and the NAD(P)$^+$ oxidant. Importantly, we observed that intracellularly captured **SCHO** remained unaffected by ABC transporter activity. As a result, **SCHO** exhibited selective phototoxicity in ALDH^{High} TNBC cells (e.g., MDA-MB-231) compared to ALDH^{Low} cells by generating superoxide radicals ($O_2^{-\bullet}$) under white LED lamp irradiation. Moreover, it was interesting to find that **SCHO** could induce CSC cell apoptosis and pyroptosis by activating the caspase-3/gasdermin E pathway.[29] Furthermore, we observed that **SCHO**-mediated PDT not only decreased the population of ALDH^{High} cancer cells but also altered tumor heterogeneity and drug resistance by lowering stemness characteristics. Last, combination therapy **SCHO** with 5-fluorouracil (5-FU) overcame chemotherapy resistance with 5-FU. This study represents the first proof-of-concept of cellular metabolism–based PS accumulation. Our findings present a novel CSC-targeting strategy by designing PDT agents that satisfy both CSC-overexpressing enzyme substrates and non-ABC transporter substrates.

RESULTS AND DISCUSSION

Design, Synthesis, and Characterization of SCHO

The ALDH-responsive PS **SCHO** was designed by tethering a thionylated coumarin-based PS to 4-aminomethyl benzaldehyde as the ALDH recognition group (Figure 1B). To enhance the triplet yield and mitigate dark toxicity concerns, a heavy atom–free strategy substituting oxygen atoms with sulfur atoms) was used (Figure 1B).[30,31] All synthetic routes are illustrated in Schemes 1S and 2S. Lawesson's reagent was used to prepare thionylated coumarin **6** as the PS. One terephthalaldehyde aldehyde was protected by an acetal functional group, while the other aldehyde was employed to create a secondary amine through reductive amination to yield **3**. Subsequently, an azide moiety was introduced to form **4**, which underwent a click reaction with *N*-propargylated coumarin to synthesize **7**. Subsequent hydrolysis yielded **SCHO**. To confirm that **SCHO** yields a carboxylate product upon incubation with ALDH, we synthesized **SCOOH**, an enzymatic product of ALDH. The ester was hydrolyzed under basic conditions, followed by a click reaction with **6**, i.e., the obtained **SCOOH**. All new compounds were characterized by ^{1}H NMR, ^{13}C NMR, and ESI-MS; the results are provided in (Figures S1–24).

https://doi.org/10.1021/jacsau.4c00642
JACS Au 2024, 4, 3657–3667

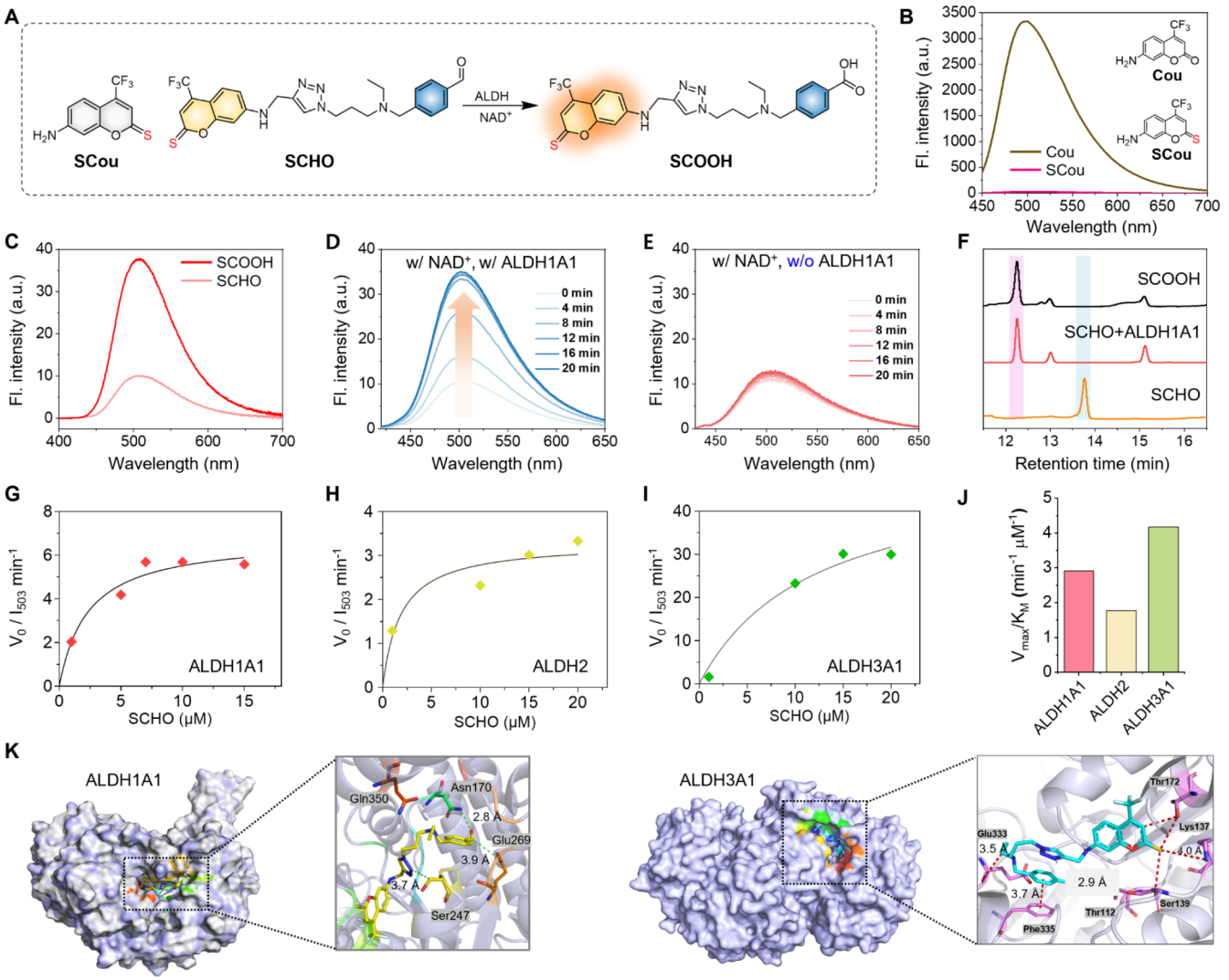

Figure 2. SCHO as an ALDH substrate. (A) Chemical structures of **SCHO** and the proposed activation mechanism in the presence of ALDH with the cofactor NAD^+. (B) Fluorescence spectra of Cou and **SCou** (10 μM, λ_{ex} = 385 nm). (C) Fluorescence spectra of **SCHO** (10 μM) and the synthetically prepared **SCOOH** (10 μM). (D) The fluorescence spectra of **SCHO** (10 μM) were recorded every 4 min after incubating with ALDH1A1 (3.3 μg/mL) and NAD^+ (1 mM) for up to 20 min. (E) Fluorescence spectra of SCHO (10 μM) with NAD^+ (1 mM) but without ALDH1A1. All samples are measured in tris buffer (pH 7.5) with 1% DMSO at 37 °C. (F) HPLC analysis (absorbance at 254 nm) of 10 μM **SCHO** before and after incubation with 3.3 μg/mL ALDH1A1 and 500 μM NAD^+ at 37 °C for 30 min. The chromatograms of **SCHO** and **SCOOH** are also presented. (G) Time-dependent increase in the fluorescence of **SCHO** at 503 nm upon incubation with ALDH1A1 (3.3 μg/mL) and NAD^+ (1 mM), ALDH2 (3.3 μg/mL) and NAD^+ (1 mM), or ALDH3A1 (3.3 μg/mL) and $NADP^+$ (1 mM) in tris buffer (pH 7.5) at 37 °C. Kinetic studies of the **SCHO** reaction under (G) ALDH1A1, (H) ALDH2, and (I) ALDH3A1 with varying concentrations of **SCHO**. (J) Kinetic parameters for **SCHO** with ALDH isoforms. (K) Calculated binding of **SCHO** with ALDH1A1 (PDB ID: 4WB9) and ALDH3A1 (PDB ID: 3SZA).

Figure 2A illustrates the assessment of PS **SCHO** as an ALDH substrate and demonstrates the proposed ALDH1A1-mediated oxidation of **SCHO** to **SCOOH**. The corresponding reference PS, **SCou**, was designed for comparison. The optical properties of **SCou**, **SCHO**, and **SCOOH** were analyzed by measuring their absorbance and fluorescence spectra. Both **SCou** and **SCHO** exhibit similar broadband absorptions centered at ~450 nm (Figure S25). The fluorescence intensity of **SCou** was considerably lower than that of the coumarin scaffold, i.e., **Cou** (Figure 2B), which is attributed to the increase in triplet population through intersystem crossing (ISC) mediated by "S" atom substitution.[32,33] Then, the sensing ability of **SCHO** toward ALDH was investigated.

Concentration-dependent fluorescence intensities of **SCHO** were measured from 1 to 20 μM, and its intensity at 503 nm showed linearity with a fair R^2 value (0.991) in this concentration range (Figure S26). By comparing the fluorescence spectrum of prepared **SCOOH** with that of a carboxylate embracing the oxidized form of **SCHO** in PBS, **SCHO** fluorescence was weaker than **SCOOH** (Figure 2C). It is manifested that the fluorescence intensity of **SCHO** increased to 3-fold after the aldehyde oxidation by incubating with ALDH1A1 and NAD^+ (Figure 2D). When ALDH1A1 is absent, almost no fluorescence change was observed in **SCHO**, even in the presence of the oxidant NAD^+ (Figure 2E). These observations led us to infer putative **SCHO** enzymatic oxidation by the ALDH1A1 enzyme.

We chose to examine the enzyme kinetics of **SCHO** for ALDH1A1, ALDH2, and ALDH3A1, among the 19 isoforms of ALDH, as they are commonly expressed in human cancer.[28]

https://doi.org/10.1021/jacsau.4c00642
JACS Au 2024, 4, 3657−3667

ALDH1A1 is found in the cytosol, while ALDH2 is expressed in the mitochondrial matrix, contributing to the elimination of lipid peroxidase byproducts.[34] ALDH3A1 is expressed in both the nucleus and cytosol, metabolizing aromatic and aliphatic aldehydes.[35] Even with the Aldefluor assay that indicated that ALDH1A1 is not the sole ALDH isozyme responsible for Aldefluor oxidation, various ALDH isoforms are also indicated in this process.[36]

Recombinant ALDH2 and ALDH3A1 were exploited and compared with the activity of ALDH1A1 in a physiological solution. As shown in Figure 2C and E, the increase in fluorescence at 500 nm indicated the conversion of **SCHO** into **SCOOH**. The enzymes were incubated with **SCHO** at a concentration range of 1−20 μM as the fluorescence intensity was linear in that range (Figure S26). For ALDH1A1, **SCHO** exhibited a linear increase in fluorescence intensity up to 8 min, except at a 1 μM concentration, which reached fluorescence intensity saturation in 12 min (Figure S27). ALDH2 oxidized **SCHO** to some degree but not as efficiently as ALDH1A1 (Figure S28). The most prominent kinetics were observed for ALDH3A1, in which linearity was not observed after 2 min of incubation (Figure S29). Based on the enhanced fluorescence, the kinetic parameters were determined from the Michaelis−Menten plot (Figure 2G-I). The Michaelis−Menten constant (K_M) and V_{max} values were obtained, and the V_{max}/K_M values were calculated to compare enzyme efficiency (Table S1 and Figure 2J). These three isoforms are responsible for **SCHO** metabolism. However, ALDH1A1 and ALDH3A1 are typically active in **SCHO** oxidation. Given that ALDH1A1 and 3A1 enzymes contribute to anticancer drug resistance,[37] **SCHO** could be a potential CSC-selective PS that can yield favorable therapeutic outcomes, especially when combined with chemotherapy. Molecular docking was used to assess the experimental data. **SCHO** exhibits good binding affinity with ALDH1A1 and ALDH3A1 with thermodynamically favorable binding energies of −10.1 and −9.7 kcal/mol, respectively (Figure 2K).

High-performance liquid chromatography (HPLC) was performed to confirm the chemical structural changes in **SCHO** to **SCOOH**. After **SCHO** was exposed to the same conditions as those in the model solution experiments, a certain peak change was observed (Figure 2F). The retention time of the new peak (12.3 min) was correlated with that of the **SCOOH** peak. In addition, high-resolution mass analysis was performed on the newly presented peak 12.3 min after elution, and the exact mass of the structure (i.e., $[M+1]^+$ 546.1770 for **SCOOH**) is shown (Figure S30). These findings validate ALDH1A1-mediated oxidation, resulting in the incorporation of the **SCHO** aldehyde functional group into the carboxylate (**SCOOH**).

ROS Generation by Photoirradiating SCHO and SCOOH

Type I PSs capable of generating $O_2^{-\bullet}$ are compatible with hypoxia through superoxide dismutase-mediated disproportionation, which has gained considerable attention in terms of low O_2-dependent PDT.[15,38,39] Consequently, we assessed the ability of **SCHO** to act as an ALDH-activated $O_2^{-\bullet}$ generator. A specific fluorescent probe, dihydrorhodamine (DHR123), was used to sense the generation of aqueous $O_2^{-\bullet}$. As expected, relatively lower $O_2^{-\bullet}$ generation was observed for **SCHO** after light irradiation at 10 s intervals (Figure S31). However, when ALDH was present (e.g., ALDH1A1), the incubated **SCHO** solution exhibited a significant increase in the DHR123 absorbance (Figure 3A and B). This indicates that $O_2^{-\bullet}$ is more efficiently generated when the aldehyde **SCHO** is

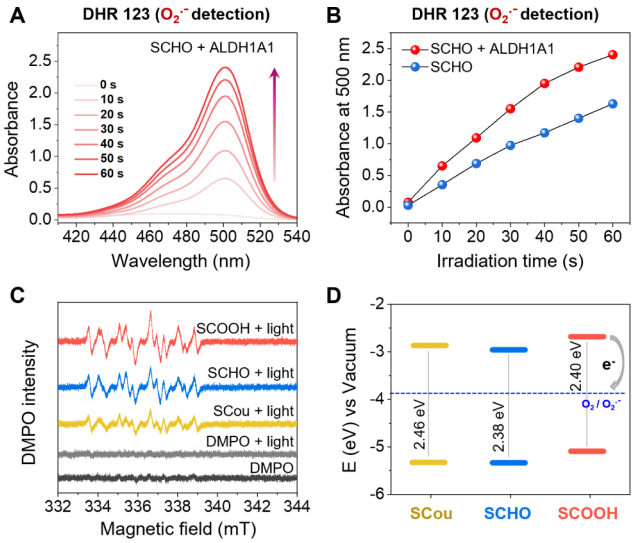

Figure 3. (A) $O_2^{-\bullet}$ detection using DHR123 (80 μM) as the specific probe, and the light was irradiated every 10 s (10 mW/cm^2). **SCHO** (10 μM) was preincubated for 30 min with ALDH1A1 (3.3 μg/mL) and NAD^+ (1 mM) in tris buffer (pH 7.5). (B) Comparison of DHR123 absorbance intensity at λ = 500 nm over time with light irradiation, based on the presence or absence of ALDH1A1 enzyme. (C) EPR spectra of PSs in DMPO measured after light irradiation. (D) Calculated HOMO, LUMO energy, and band gap of each PS to compare with the redox potential of the $O_2/O_2^{-\bullet}$.

oxidized to the carboxylate **SCOOH**. Negligible changes were observed with light-irradiated DHR123 as a control (Figure S32). Next, the **SCHO** generation of singlet oxygen ($^1O_2$) upon light irradiation using 9,10-anthracenediylbis-(methylene)-dimalonic acid (ABDA) as the $^1O_2$ trapper was attempted. The $^1O_2$ produced exhibited little change in the absorbance spectra of the ABDA indicator, even in the presence of ALDH (Figure S33). These results suggest that the designed thionylated PSs produced $^1O_2$ in low yields, indicating a preference for type-I electron transfer from an excited triplet PS* to ground-state oxygen rather than a competitive type-II energy transfer process.[15,40] The $O_2^{-\bullet}$-generating propensity was further demonstrated by measuring the electron paramagnetic resonance (EPR) spectra with the radical trap DMPO (Figure S34). The results confirmed that thionylated coumarins acted as type-I PSs, with **SCOOH** exhibiting the best performance among **SCou** and **SCHO** (Figure 3C).

Considering the preference for type-I electron transfer observed in our thionylated coumarin PSs, we conducted cyclic voltammetry using Ag/AgCl as the reference electrode to determine the redox potential of the developed PSs (Figure S35). For the oxidation process, the potential HOMO levels were calculated as −5.33 eV (**SCou**), −5.52 eV (**SCHO**), and −5.08 eV (**SCOOH**) versus the vacuum level. By combining this information with the UV−vis data, we constructed HOMO and LUMO diagrams of the PSs for visual comparison with the redox potential of $O_2/O_2^{-\bullet}$ (Figure 3D). The larger energy difference (ΔE) between LUMO and the redox potential of $O_2/O_2^{-\bullet}$ indicates a more preferable reduction process,[41] and the highest LUMO energy of **SCOOH** supports

https://doi.org/10.1021/jacsau.4c00642
JACS Au 2024, 4, 3657−3667

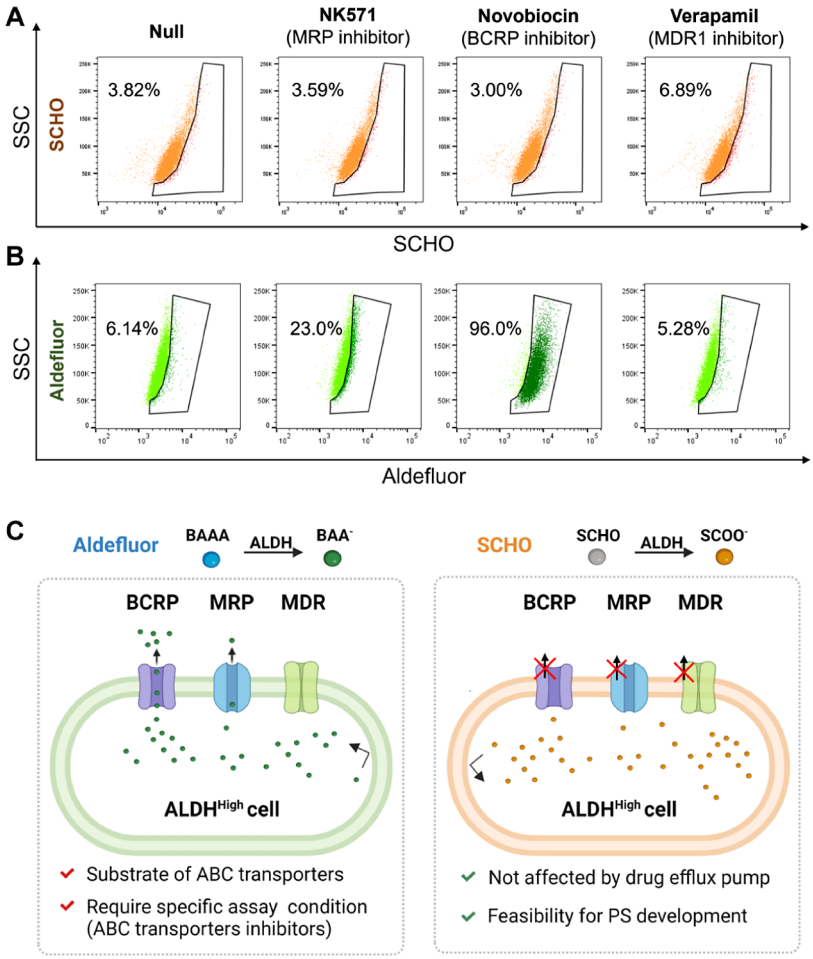

Figure 4. ABC transporters affect Aldefluor but not **SCHO**. Flow cytometry analysis of (A) **SCHO**- and (B) Aldefluor-treated MDA-MB-231 cells in the presence of MRP (MK571, 50 μM), MDR1 (verapamil, 20 μM), and BCRP (Novobiocin, 200 μM) inhibitors, as well as in the absence (null) of inhibitors. Assays are analyzed in PBS with 2% FBS. (C) Schematic diagram comparing the influence of ABC transporters on ALDH substrate fluorophores.

the optimal type-I electron transfer–mediated $O_2^{-\bullet}$ generation.

SCHO is Not a Substrate of ABC Transporters

Although ALDH1 is acknowledged as a dependable marker for cancer stemness, numerous cancer cells displaying high ALDH activity concurrently express ABC transporters, which are responsible for the efflux of drugs or metabolites.[42] In our prior research, we identified a substantial elevation of multiple drug resistance (MDR) family members (MDR1, MRP2, and BCRP) in ALDH^{High} MDA-MB-231 cells.[43] Coexpression of these transporters raises concerns regarding the potential efflux of metabolized probes, posing challenges for effective PS accumulation in the elimination of ALDH-positive cells.[27] To investigate this matter, we assessed whether **SCHO** is affected by ABC transporters in the presence of specific inhibitors: verapamil (MDR1 inhibitor), MK-571 (MRP1/2 inhibitor), and novobiocin (BCRP inhibitor). Cellular staining with **SCHO** revealed minimal differences in the presence of various ABC transporter inhibitors (Figure 4A). Since the intracellular entrapment strategy based on ALDH activity was inspired by the commercial fluorescent dye Aldefluor, we conducted the same experiment with Aldefluor to examine its effect on ABC transporters. In contrast to **SCHO**, the population of Aldefluor-stained cells increased in the presence of BCRP and MRP1/2 inhibitors (Figure 4B). These results suggested that **SCHO** is not a substrate for ABC transporters, whereas Aldefluor can be pumped out through BCRP and MRP1/2 (Figure 4C). These findings support the feasibility of using **SCHO** as a PS that selectively accumulates in CSCs with high ALDH expression levels.

Selective Accumulation of SCHO by ALDH Activity

A cell viability assay was conducted to assess the darkness and phototoxicity of **SCou** and **SCHO** in the MDA-MB-231, BT549, and MCF7 breast cancer cell lines. Both molecules exhibited no dark toxicity up to 50 μM, and **SCHO** demonstrated effective anticancer effects in all cell lines (Figures 5A and S36). This demonstrates the capability of noninvasive photodynamic therapy by focusing light irradiation on a specific targeted region. Given the higher discriminative phototoxicity of **SCHO** compared to that of **SCou** in MDA-MB-231 cells, we decided to delve deeper into MDA-MB-231 cells. Considering that ALDH1A1 is a representative cancer stemness marker in MDA-MB-231 cells,[44] we anticipated that type-I PDT using **SCHO** would be beneficial for the accumulation and production of ROS in ALDH-active breast CSCs. The effective accumulation principles of **SCHO** and **SCou** in ALDH^{High} cells are compared in Figure 5B. *In vitro* fluorescence of **SCou**, **SCHO**, and **SCOOH** was measured,

https://doi.org/10.1021/jacsau.4c00642
JACS Au 2024, 4, 3657−3667

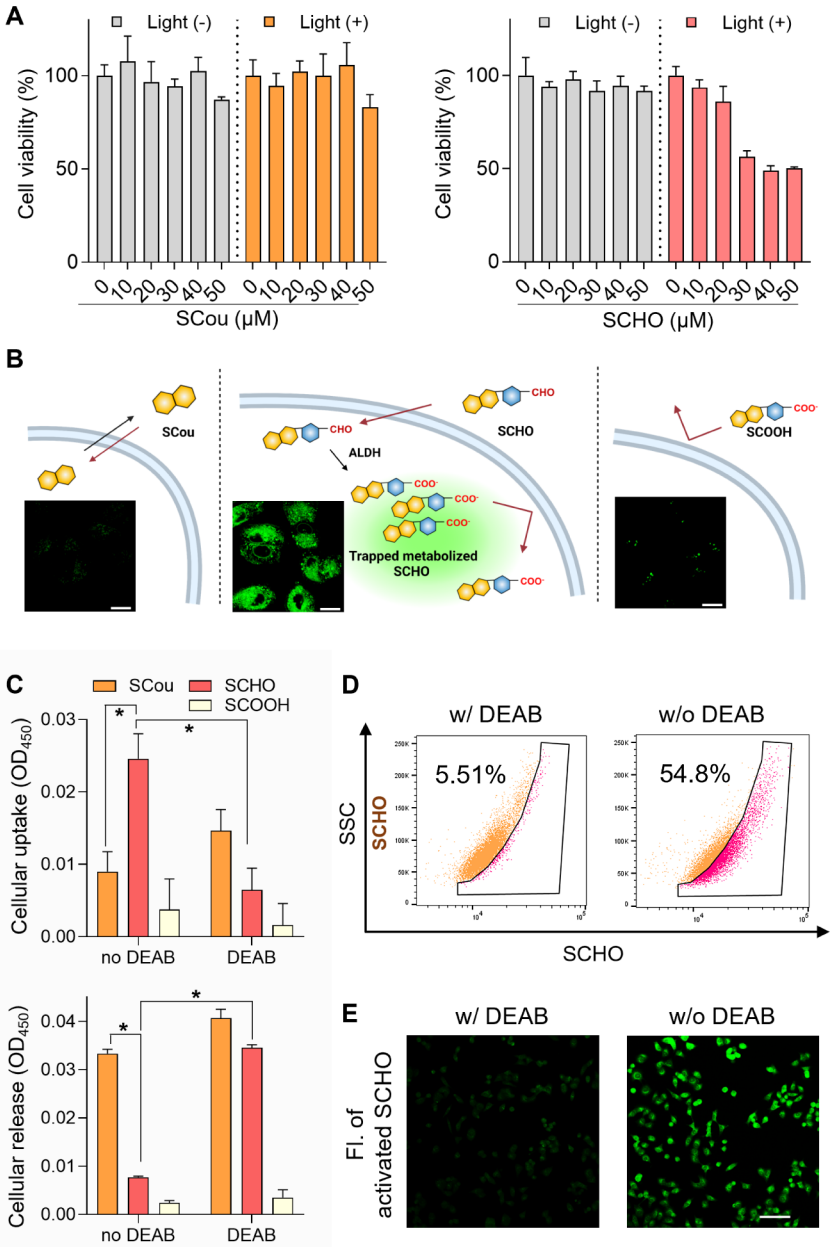

Figure 5. (A) Viability of MDA-MB-231 cells treated with **SCou** or **SCHO** (0−50 μM) under dark or photoirradiation conditions after 24 h (white light, 10 mW/cm^2). (B) Illustration of the principle of **SCHO** accumulation in ALDH-expressing cells and CLSM imaging of each compound (50 μM)−treated MDA-MB-231 cell. Scale bar: 15 μm. (C) Cellular uptake and release of **SCou**, **SCHO**, and **SCOOH** in MDA-MB-231 cells. (D) Flow cytometry analysis of **SCHO**-treated MDA-MB-231 with or without DEAB (ALDH inhibitor). (E) In vitro live cell fluorescence imaging of **SCHO** (50 μM)−treated MDA-MB-231 cells with or without DEAB (1 mM). Scale bar: 100 μm.

showing definite accumulation of **SCHO**, whereas negligible fluorescence was observed in **SCou**- and **SCOOH**-treated MDA-MB-231 cells (Figure 5B). The intracellular uptake of **SCou**, **SCHO**, and **SCOOH** by MDA-MB-231 cells was compared by measuring the absorbance before and after 2 h of incubation. As expected, the cells absorb more **SCHO** than **SCou**, and a significant reduction in uptake was observed in the DEAB-pretreated cells (DEAB is an ALDH inhibitor; see Figure 5C). The same was true for PS release, where a large amount of **SCHO** penetrated DEAB-pretreated ALDH-inhibited cells, supporting our assumption that **SCHO** is metabolized by ALDH and trapped inside the cells. Flow cytometry analysis of **SCHO**-treated MDA-MB-231 cells with or without the ALDH inhibitor DEAB confirmed that ALDH activity affected **SCHO** accumulation (Figure 5D). Confocal laser scanning microscopy (CLSM) imaging further supported **SCHO** accumulation in ALDH-active cells (Figure 5E).

SCHO-Mediated Type-I PDT Induces CSC-like Cell Apoptosis and Pyroptosis

Calcein-AM/PI staining provided intuitive validation that **SCHO** accumulated and elicited a superior phototherapeutic response compared to that of **SCou** in CSC-like MDA-MB-231 cells (Figure 6A). To investigate apoptotic cell populations, Annexin V/PI−stained cells were analyzed by flow cytometry, which distinctly revealed early and late apoptotic cells in light-irradiated **SCHO**-treated cells (Figures 6B and S37). Some necrotic cells were observed in light irradiated groups, assumed to be due to the high concentration of photosensitizer. We

https://doi.org/10.1021/jacsau.4c00642
JACS Au 2024, 4, 3657−3667

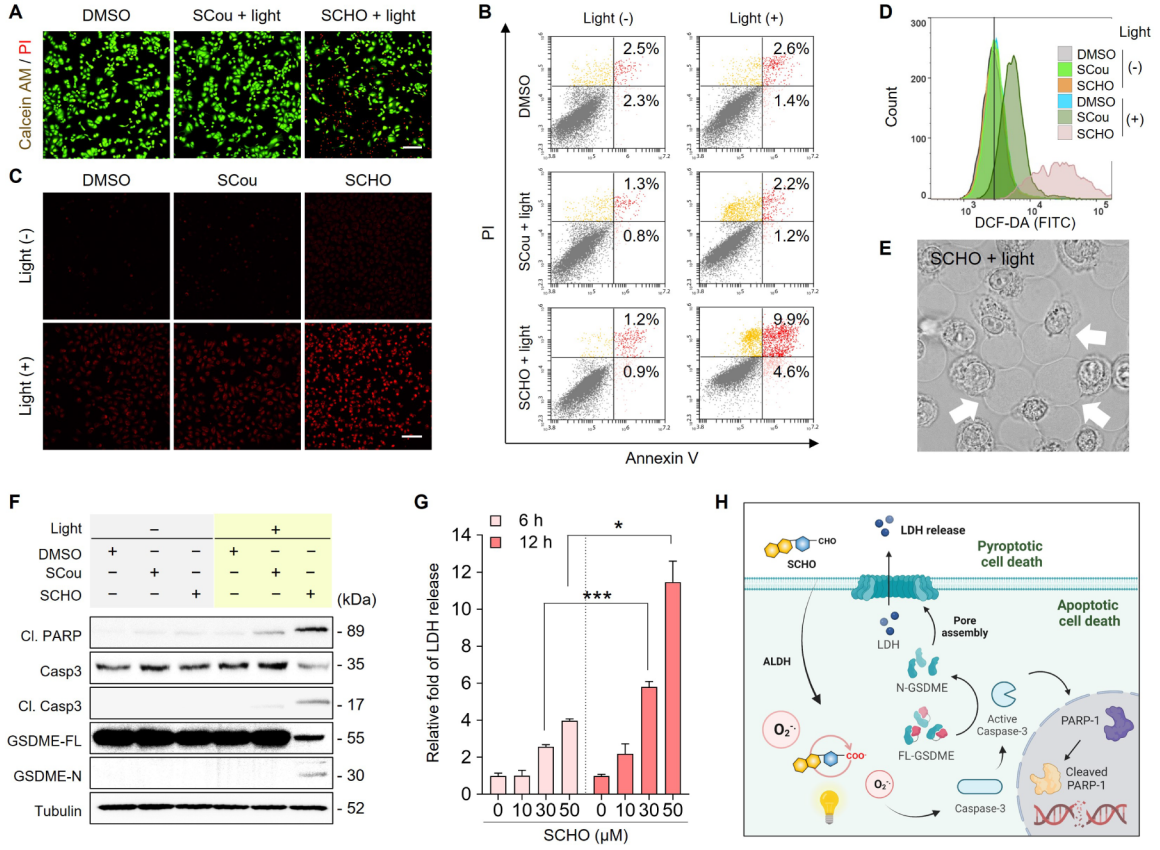

Figure 6. (A) Confocal imaging of **SCou** or **SCHO** (50 μM)−treated MDA-MB-231 cells after photoirradiation. Live cells were stained with calcein-AM (green), while dead cells were stained with phosphoric acid (PI) (red). Scale bar: 100 μm. (B) Flow cytometry analysis using Annexin V-FITC and propidium (PI) of MDA-MB-231 cells treated with **SCou** or **SCHO** (50 μM) 24 h after photoirradiation (white light, 25 mW/cm^2, 10 min). (C) Confocal imaging of intracellular $O_2^{-\bullet}$ production under dark or light irradiation using DHE (10 μM) staining dye. Scale bar: 100 μm. (D) Flow cytometry analysis for DCFH-DA−stained MDA-MB-231 cells to show the ROS levels. MDA-MB-231 cells are treated with **SCou** or **SCHO** (50 μM) for 2 h before photoirradiation (white light, 25 mW/cm^2, 10 min). (E) Magnified cellular images used to visualize the morphologic changes. Scale bar: 100 μm. (F) Western blot analysis of the cleavage of PARP-1, caspase-3, and GSDME from MDA-MB-231 cells after treating with **SCou** or **SCHO** (50 μM) under conditions of dark or light irradiation (white light, 25 mW/cm^2, 10 min). (G) Lactate dehydrogenase (LDH) release from MDA-MB-231 cells treated with **SCHO** (0−50 μM) under conditions of photoirradiation (white light, 10 mW/cm^2, 10 min), which was assayed after 6 and 12 h. (H) Schematic illustration of the proposed combinatory pyroptotic and apoptotic cell death via accumulated and metabolized **SCHO**.

aimed to enhance PDT efficiency using **SCHO** to retain more photosensitizers within the cells. This approach, indicated by increased Annexin V and PI signals, suggests that our method effectively shifts cell fate more toward apoptosis and pyroptosis. Poly(ADP-ribose) polymerase (PARP) plays a crucial role in genome stability and DNA repair, and cleaved PARP indicates the induction of apoptosis in cancer cells.[7] When MDA-MB-231 cells were photoirradiated after **SCHO** treatment, Western blot analysis revealed elevated levels of cleaved apoptosis-associated PARP and caspase-3 (Figures 6F and S38). These results demonstrate that **SCHO** induces apoptosis much more effectively than **SCou** at the same concentration, attributed to the ALDH enzyme activity, facilitating **SCHO** accumulation in the cytosol. Supported by the ROS fluorescence probes and EPR results shown in Figure 4, light irradiation−mediated $O_2^{-\bullet}$ generation in CSCs was also visualized using dihydroethidium (DHE) staining. DHE signals were observed only in light-irradiated **SCHO**-treated cells, indicating that **SCHO** successfully accumulated and produced $O_2^{-\bullet}$ in MDA-MB-231 cells (Figure 6C). Flow cytometry using DCFH-DA, an ROS-staining dye, further confirmed that **SCHO** induced an increased level of ROS accumulation in cells (Figures 6D and S39).

Pyroptosis, a programmed cell death associated with inflammation, relies on gasdermin protein families.[45,46] Hyper-accumulation of intracellular ROS is known to be associated with caspase-3/GSDME-dependent pyroptosis.[39,47,48] Notably, CSC-like **SCHO**-treated cells displayed characteristic pyroptosis-like morphological changes during type I PDT treatment, including cell swelling, formation of large bubbles in the membrane, and intact nuclei (Figure 6E).[45,46] Accordingly, a Western blot assay was performed to examine the cleavage of GSDME or GSDMD. Cleaved caspase-3 and the *N*-terminal fragment (GSDME-N) were observed in photoirradiated **SCHO**-treated MDA-MB-231 cells, whereas none of the other dark- or light-irradiated **SCou** groups showed these cleaved forms (Figures 6F). The concentration-dependent release of pyroptosis markers, including lactate dehydrogenase (LDH), from photoirradiated **SCHO**-treated cells further supported the formation of GSDME pores and membrane lysis, resulting in LDH leakage into the extracellular fluid compartment (Figure 6G), suggesting pyroptotic cell death. Collectively, these findings highlight that **SCHO**-induced

https://doi.org/10.1021/jacsau.4c00642
JACS Au 2024, 4, 3657−3667

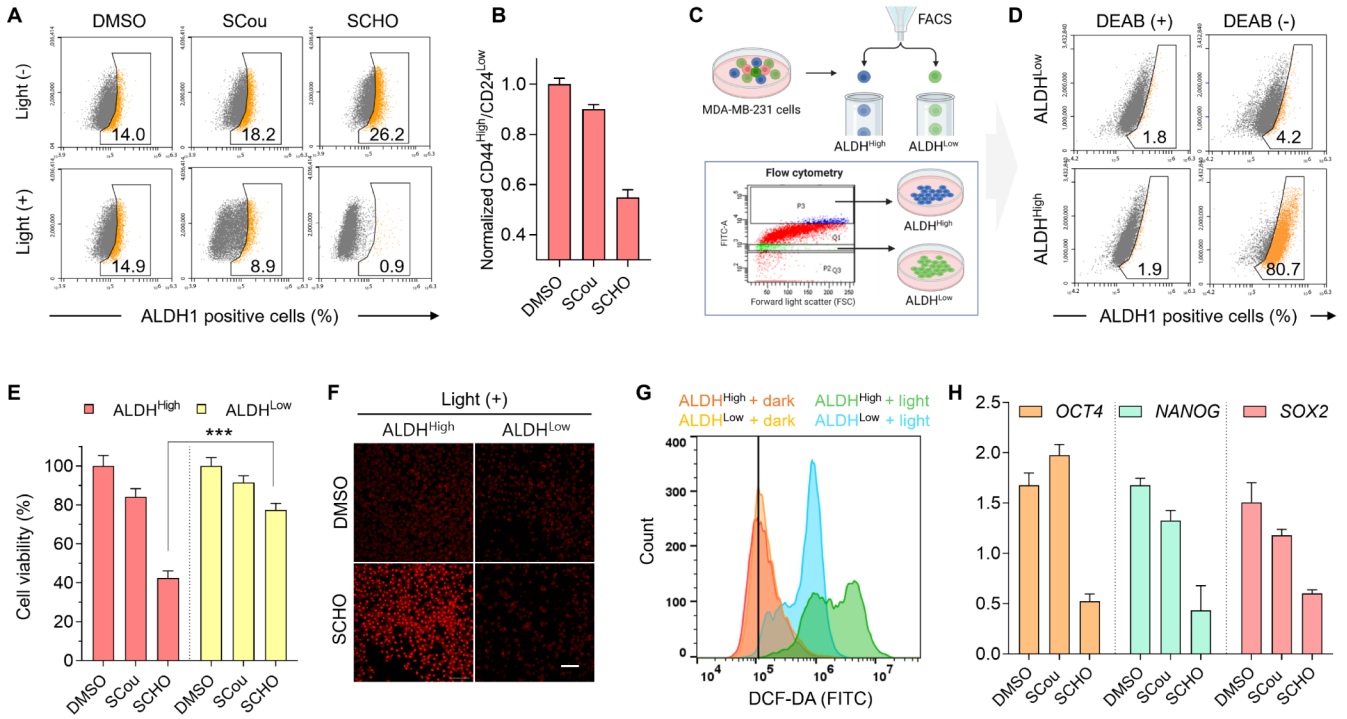

Figure 7. Investigation of ALDH population decreases by type-I PDT with SCHO. (A) Photodynamic effect of the test compounds on ALDH1 activity by an Aldefluor assay. Diethylaminobenzaldehyde (DEAB, a specific ALDH1 inhibitor) was used to define the Aldefluor-positive phenotype. (B) $CD44^{High}/CD24^{Low}$ populations determined by flow cytometry. (C) Description of $ALDH1^{High}$ and $ALDH1^{Low}$ cells by FACS. (D) Flow cytometry analysis for measuring ALDH1 activity in $ALDH1^{High}$ and $ALDH1^{Low}$ MDA-MB-231 cells. (E) Cell viability after PDT in $ALDH1^{High}$ and $ALDH1^{Low}$ MDA-MB-231 cells. (F) Confocal imaging of induced $O_2^{-\bullet}$ production under DMSO or **SCHO** followed by light irradiation in $ALDH^{High}$ and $ALDH^{Low}$ MDA-MB-231 cells. Scale bar: 100 μm. (G) Flow cytometry analysis of ROS accumulation by the DCFH-DA indicator. (H) mRNA levels of CSC markers of human OCT4, NANOG, and SOX2 in MDA-MB-231 cells treated with 50 μM compounds followed by photoirradiation (white light, 25 mW/cm^2, 10 min).

photodynamic cell death involves a synchronized combination of apoptotic and pyroptotic cell death; as illustrated in Figure 6H.

Study of CSC-like Characteristics Decrease After SCHO-Mediated Type-I PDT

Encouraged by the accumulation of the **SCHO** metabolic product **SCOOH** and the induction of cell death in MDA-MB-231 cells after light irradiation, we evaluated whether selective type-I PDT with **SCHO** removed cells with higher ALDH activity, thereby reducing the characteristics of cancer stemness in the cell population. The Aldefluor flow cytometry assay,[49] which is widely used to investigate ALDH-active cell populations, was performed. Based on the findings presented in Figure 6 and a previous report indicating that ALDH1A1, 2, and 3A1 are active ALDH isoforms in the Aldefluor assay, we hypothesized that **SCHO**-mediated photodynamic cell death resulted in a reduction of the ALDH-active population. MDA-MB-231 cells were pretreated with 50 μM **SCou** and **SCHO**, and white LED lamp light was irradiated for 10 min. Pretreated and light-irradiated **SCHO** cells exhibited a remarkable decrease in the fraction of $ALDH^{High}$ cells in their heterogeneous population (Figure 7A). Along with ALDH activity, $CD44^{High}/CD24^{Low}$ is a breast CSC (BCSC) marker correlated with a lower overall survival rate in patients.[50,51] Exposure to **SCHO** and light irradiation significantly reduced the $CD44^{High}/CD24^{Low}$-harboring population in MDA-MB-231 cells compared to **SCou** (Figures 7B and S40).

To further establish the selective accumulation and activation of **SCHO** in ALDH-active cells, we sorted $ALDH^{High}$ and $ALDH^{Low}$ cells through fluorescence-activated cell sorting (FACS) using the Aldefluor kit (Figure 7C). As anticipated, the photodynamic effect of **SCHO** was significantly greater in $ALDH^{High}$ cells (Figure 7D). Using the same analysis method as that shown in Figure 5C, we compared the uptake of **SCHO** by $ALDH^{High}$ and $ALDH^{Low}$ cells (Figure S41). As expected, more **SCHO** accumulated in $ALDH^{High}$ cells than in $ALDH^{Low}$ cells. We measured the fluorescence of the photosensitizer in lysate after compound treatment in unsorted MDA-MB-231 cells and $ALDH^{High}$ cells and $ALDH^{High}$ cells exhibited higher fluorescence intensity than that of unsorted cells, implying the higher efficiency of accumulation as well as the conversion to **SCOOH** (Figure S42). We analyzed and compared early and late apoptosis in sorted MDA-MB-231 cells after **SCou** and **SCHO** challenges. Significant difference in the apoptotic cell populations was observed in **SCHO**-treated and photoirradiated $ALDH^{High}$ and $ALDH^{Low}$ cells, whereas few differences were observed in **SCou**-treated cells (Figure S43). Consistent with these results, a marked difference was observed in **SCHO**-mediated $O_2^{-\bullet}$ production between $ALDH^{High}$ and $ALDH^{Low}$ cells, as analyzed by DHE-stained live-cell CLSM imaging and flow cytometry using DCFH-DA (Figure 7F,G). Photoirradiation in the presence of **SCHO** significantly reduced the expression of stemness marker genes (OCT4, NANOG, and SOX2), which are criteria for CSCs (Figure 7H). Notably, little suppression of stemness characteristics was observed in the **SCou** photoirradiated cells (control), confirming our hypothesis that ALDH activity–based metabolism and trapping of **SCHO** could successfully decrease the

https://doi.org/10.1021/jacsau.4c00642
JACS Au 2024, 4, 3657−3667

population of CSCs and alter tumor heterogeneity through photoirradiation.

As ALDH^{High} cancer cells show augmented DNA damage and oxidative stress response pathways,[52] we hypothesized that 5-fluorouracil (5-FU) treatment of MDA-MB-231 cells could increase the ALDH^{High} population. As shown in Figure 8A, a

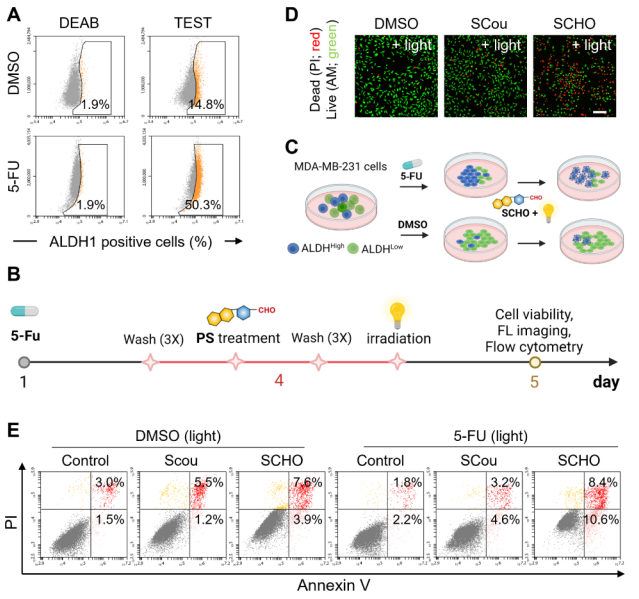

Figure 8. (A) Flow cytometry analysis of ALDH1 activity for 5-FU (500 μM) or DMSO-treated MDA-MB-231 cells. (B) Scheme of the investigating **SCHO** photodynamic effects of 5-FU (500 μM) that survived MDA-MB-231 cells. MDA-MB-231 cells were exposed to 5-FU (500 μM) for 3 days in fresh medium and subsequently received photodynamic therapy. (C) Depiction of an augmenting PDT effect in combination with 5-FU chemotherapy. (D) Confocal imaging of **SCou**- or **SCHO** (50 μM)−treated 5-FU pretreated MDA-MB-231 cells after photoirradiation. (E) Flow cytometry analysis to measure apoptosis in 5-FU−pretreated MDA-MB-231 cells subjected to photodynamic therapy. DMSO is treated as a negative control.

distinct increase in the ALDH^{High} population suggests that cells with high ALDH activity are likely to exhibit resistance to the chemotherapeutic drug 5-FU. Encouraged by this result, we decided to explore **SCHO** type-I PDT as a means to overcome 5-FU resistance. The cells were pretreated with 5-FU, and the surviving cells were subjected to photoirradiation in combination with DMSO, **SCou**, or **SCHO** (Figure 8B). As expected, the number of apoptotic cells increased in **SCHO** photoirradiated with 5-FU pretreated cells (Figure 8C−E). This suggests that the application of **SCHO** may be further extended to treatment-resistant cancer cells associated with ALDH activity.

CONCLUSION

In summary, we developed a thionylated coumarin-based ALDH substrate, type-I PS, **SCHO**, and successfully demonstrated that the enzymatic metabolism of **SCHO** could facilitate selective uptake and accumulation in ALDH^{High} MDA-MB-231 cells, resulting in the induction of both apoptosis and pyroptosis after PDT. This study highlights a clear distinction between ALDH inhibitors that inhibit only ALDH enzyme activity. **SCHO**-mediated PDT reduced the population of ALDH-overexpressing cells. The design of an ALDH enzyme substrate photosensitizer is unaffected by drug efflux pumps such as ABC transporters because the nature of the **SCHO** metabolite (**SCOOH**) remains unaffected. Additionally, we demonstrated that eliminating ALDH^{High} cells through type-I PDT could reduce the stemness of the remaining cells. Consequently, we observed a reduction in the cancer stemness of MDA-MB-231 cell population after PDT with **SCHO**. Therefore, we believe that **SCHO** can be used for further studies on outcomes after eliminating ALDH^{High} cells. Our photosensitizer design, which specifically targets high-activity ALDH enzyme cells, can effectively expand selective photosensitizer delivery strategies.

ASSOCIATED CONTENT

Supporting Information

The Supporting Information is available free of charge at https://pubs.acs.org/doi/10.1021/jacsau.4c00642.

Detailed experimental conditions and methods, synthesis, structural characterization, subcellular localization, and functional characterization for biological evaluation (PDF)

AUTHOR INFORMATION

Corresponding Authors

Mingle Li − *College of Materials Science and Engineering, Shenzhen University, Shenzhen 518060, China;* orcid.org/0000-0002-0384-9128; Email: limingle@szu.edu.cn

Jong Seung Kim − *Department of Chemistry, Korea University, Seoul 02841, Korea;* orcid.org/0000-0003-3477-1172; Email: jongskim@korea.ac.kr

Authors

Ji Hyeon Kim − *Department of Chemistry, Korea University, Seoul 02841, Korea; Department of Chemical and Systems Biology, Chem-H and Stanford Cancer Institute, Stanford School of Medicine, Stanford University, Stanford, California 94305, United States*

Jieun Lee − *Department of Chemistry, Korea University, Seoul 02841, Korea*

Kyung-Woo Lee − *Department of Chemistry, Korea University, Seoul 02841, Korea*

Hao Xiong − *Department of Chemistry, Korea University, Seoul 02841, Korea*

Complete contact information is available at: https://pubs.acs.org/10.1021/jacsau.4c00642

Author Contributions

‖J.H.K., J. L., and K.−W. L. contributed equally to this work. CRediT: **Ji Hyeon Kim** conceptualization, data curation, formal analysis, investigation, project administration, validation, writing-original draft; **Jieun Lee** data curation, formal analysis, methodology, validation; **Kyung-Woo Lee** data curation, formal analysis, validation, visualization; **Hao Xiong** resources; **Mingle Li** funding acquisition, writing-review & editing; **Jong Seung Kim** funding acquisition, supervision, writing-review & editing.

Notes

The authors declare no competing financial interest.

https://doi.org/10.1021/jacsau.4c00642
JACS Au 2024, 4, 3657−3667

■ ACKNOWLEDGMENTS

This work was supported by the Korean Creative Research Initiative (CRI project No. 2018R1A3B1052702, J.S.K.) of the National Research Foundation of Korea (NRF) funded by the Korea Ministry of Science and ICT (MSIT). M.L. wishes to thank the National Natural Science Foundation of China (Grant No. 22308220), the Shenzhen University Third-Phase Project of Constructing High-Level University (Grant No. 000001032104), and the Research Team Cultivation Program of Shenzhen University (Grant No. 2023QNT005).

■ REFERENCES

(1) Nguyen, L. V.; Vanner, R.; Dirks, P.; Eaves, C. J. Cancer stem cells: An evolving concept. *Nat. Rev. Cancer* **2012**, *12*, 133−143.
(2) Batlle, E.; Clevers, H. Cancer stem cells revisited. *Nat. Med.* **2017**, *23*, 1124−1134.
(3) Clarke, M. F. Clinical and Therapeutic Implications of Cancer Stem Cells. *New Engl. J. Med.* **2019**, *380*, 2237−2245.
(4) Phi, L. T. H.; Sari, I. N.; Yang, Y.-G.; Lee, S.-H.; Jun, N.; Kim, K. S.; Lee, Y. K.; Kwon, H. Y. Cancer Stem Cells (CSCs) in Drug Resistance and their Therapeutic Implications in Cancer Treatment. *Stem Cells Int.* **2018**, *2018*, 5416923.
(5) Baumann, M.; Krause, M.; Hill, R. Exploring the role of cancer stem cells in radioresistance. *Nat. Rev. Cancer* **2008**, *8* (7), 545−554.
(6) Han, J.; Won, M.; Kim, J. H.; Jung, E.; Min, K.; Jangili, P.; Kim, J. S. Cancer stem cell-targeted bio-imaging and chemotherapeutic perspective. *Chem. Soc. Rev.* **2020**, *49*, 7856−7878.
(7) Park, M.; Sunwoo, K.; Kim, Y.-J.; Won, M.; Xu, Y.; Kim, J.; Pu, Z.; Li, M.; Kim, J. Y.; Seo, J. H.; et al. Cutting Off H^+ Leaks on the Inner Mitochondrial Membrane: A Proton Modulation Approach to Selectively Eradicate Cancer Stem Cells. *J. Am. Chem. Soc.* **2023**, *145*, 4647−4658.
(8) Mai, T. T.; Hamaï, A.; Hienzsch, A.; Cañeque, T.; Müller, S.; Wicinski, J.; Cabaud, O.; Leroy, C.; David, A.; Acevedo, V.; et al. Salinomycin kills cancer stem cells by sequestering iron in lysosomes. *Nat. Chem.* **2017**, *9*, 1025−1033.
(9) Boodram, J. N.; Mcgregor, I. J.; Bruno, P. M.; Cressey, P. B.; Hemann, M. T.; Suntharalingam, K. Breast Cancer Stem Cell Potent Copper(II)−Non-Steroidal Anti-Inflammatory Drug Complexes. *Angew. Chem., Int. Ed.* **2016**, *55*, 2845−2850.
(10) Kim, J. H.; Verwilst, P.; Won, M.; Lee, J.; Sessler, J. L.; Han, J.; Kim, J. S. A Small Molecule Strategy for Targeting Cancer Stem Cells in Hypoxic Microenvironments and Preventing Tumorigenesis. *J. Am. Chem. Soc.* **2021**, *143*, 14115−14124.
(11) Pattabiraman, D. R.; Weinberg, R. A. Tackling the cancer stem cells - what challenges do they pose? *Nat. Rev. Drug Discovery* **2014**, *13*, 497−512.
(12) Shen, S.; Xu, X.; Lin, S.; Zhang, Y.; Liu, H.; Zhang, C.; Mo, R. A nanotherapeutic strategy to overcome chemotherapeutic resistance of cancer stem-like cells. *Nat. Nanotechnol.* **2021**, *16*, 104−113.
(13) Shen, F.-F.; Dai, S.-Y.; Wong, N.-K.; Deng, S.; Wong, A. S.-T.; Yang, D. Mediating K^+/H^+ Transport on Organelle Membranes to Selectively Eradicate Cancer Stem Cells with a Small Molecule. *J. Am. Chem. Soc.* **2020**, *142*, 10769−10779.
(14) Kim, J. H.; Park, S.; Jung, E.; Shin, J.; Kim, Y.-J.; Kim, J. Y.; Sessler, J. L.; Seo, J. H.; Kim, J. S. A dual-action niclosamide-based prodrug that targets cancer stem cells and inhibits TNBC metastasis. *P. Natl. Acad. Sci. U.S.A.* **2023**, *120*, No. e2304081120.
(15) Li, M.; Xu, Y.; Peng, X.; Kim, J. S. From Low to No O2-Dependent Hypoxia Photodynamic Therapy (hPDT): A New Perspective. *Acc. Chem. Res.* **2022**, *55*, 3253−3264.
(16) Agostinis, P.; Berg, K.; Cengel, K. A.; Foster, T. H.; Girotti, A. W.; Gollnick, S. O.; Hahn, S. M.; Hamblin, M. R.; Juzeniene, A.; Kessel, D.; et al. Photodynamic therapy of cancer: An update. *Ca-Cancer J. Clin.* **2011**, *61* (4), 250−281.
(17) Xiong, T.; Peng, Q.; Chen, Y.; Li, M.; Du, J.; Fan, J.; Jia, L.; Peng, X. A Novel Nanobody−Photosensitizer Conjugate for Hypoxia Resistant Photoimmunotherapy. *Adv. Funct. Mater.* **2021**, *31*, 2103629.
(18) Li, M.; Shao, Y.; Kim, J. H.; Pu, Z.; Zhao, X.; Huang, H.; Xiong, T.; Kang, Y.; Li, G.; Shao, K.; et al. Unimolecular Photodynamic O_2-Economizer To Overcome Hypoxia Resistance in Phototherapeutics. *J. Am. Chem. Soc.* **2020**, *142*, 5380−5388.
(19) Koo, S.; Lee, M.-G.; Sharma, A.; Li, M.; Zhang, X.; Pu, K.; Chi, S.-G.; Kim, J. S. Harnessing GLUT1-Targeted Pro-oxidant Ascorbate for Synergistic Phototherapeutics. *Angew. Chem., Int. Ed.* **2022**, *61*, No. e202110832.
(20) Lucky, S. S.; Soo, K. C.; Zhang, Y. Nanoparticles in Photodynamic Therapy. *Chem. Rev.* **2015**, *115*, 1990−2042.
(21) Vasiliou, V.; Pappa, A.; Estey, T. Role of human aldehyde dehydrogenases in endobiotic and xenobiotic metabolism. *Drug Metab. Rev.* **2004**, *36*, 279−299.
(22) Li, X.; Higashikubo, R.; Taylor, J.-S. Use of multiple carboxylates to increase intracellular retention of fluorescent probes following release from cell penetrating fluorogenic conjugates. *Bioconjugate Chem.* **2008**, *19*, 50−56.
(23) Salam, R.; Chowdhury, S. M.; Marshall, S. R.; Gneid, H.; Busschaert, N. Increasing membrane permeability of carboxylic acid-containing drugs using synthetic transmembrane anion transporters. *Chem. Commun.* **2021**, *57*, 13122−13125.
(24) Toledo-Guzmán, M. E.; Hernandez, M. I.; Gómez-Gallegos, Á. A.; Ortiz-Sánchez, E. ALDH as a Stem Cell Marker in Solid Tumors. *Curr. Stem Cell Res. Ther.* **2019**, *14*, 375−388.
(25) Panigoro, S. S.; Kurnia, D.; Kurnia, A.; Haryono, S. J.; Albar, Z. A. ALDH1 cancer stem cell marker as a prognostic factor in triple-negative breast cancer. *J. Surg. Oncol.* **2020**, *2020*, 7863243.
(26) Zeng, X.; Liu, C.; Yao, J.; Wan, H.; Wan, G.; Li, Y.; Chen, N. Breast cancer stem cells, heterogeneity, targeting therapies and therapeutic implications. *Pharmacol. Res.* **2021**, *163*, 105320.
(27) Park, J. W.; Jung, K.-H.; Byun, Y.; Lee, J. H.; Moon, S. H.; Cho, Y. S.; Lee, K.-H. ATP-binding cassette transporters substantially reduce estimates of ALDH-positive Cancer cells based on Aldefluor and AldeRed588 assays. *Sci. Rep.* **2019**, *9*, 6462.
(28) Pereira, R.; Gendron, T.; Sanghera, C.; Greenwood, H. E.; Newcombe, J.; McCormick, P. N.; Sander, K.; Topf, M.; Årstad, E.; et al. Mapping aldehyde dehydrogenase 1A1 activity using an [18F] substrate-based approach. *Chem. eur. J.* **2019**, *25*, 2345−2351.
(29) Wang, Y.; Gao, W.; Shi, X.; Ding, J.; Liu, W.; He, H.; Wang, K.; Shao, F. Chemotherapy drugs induce pyroptosis through caspase-3 cleavage of a gasdermin. *Nature* **2017**, *547*, 99−103.
(30) Li, M.; Xia, J.; Tian, R.; Wang, J.; Fan, J.; Du, J.; Long, S.; Song, X.; Foley, J. W.; Peng, X. Near-Infrared Light-Initiated Molecular Superoxide Radical Generator: Rejuvenating Photodynamic Therapy against Hypoxic Tumors. *J. Am. Chem. Soc.* **2018**, *140*, 14851−14859.
(31) Li, M.; Xiong, T.; Du, J.; Tian, R.; Xiao, M.; Guo, L.; Long, S.; Fan, J.; Sun, W.; Shao, K.; et al. Superoxide Radical Photogenerator with Amplification Effect: Surmounting the Achilles' Heels of Photodynamic Oncotherapy. *J. Am. Chem. Soc.* **2019**, *141*, 2695−2702.
(32) Pollum, M.; Jockusch, S.; Crespo-Hernandez, C. E. 2, 4-Dithiothymine as a potent UVA chemotherapeutic agent. *J. Am. Chem. Soc.* **2014**, *136*, 17930−17933.
(33) Nguyen, V.-N.; Qi, S.; Kim, S.; Kwon, N.; Kim, G.; Yim, Y.; Park, S.; Yoon, J. An emerging molecular design approach to heavy-atom-free photosensitizers for enhanced photodynamic therapy under hypoxia. *J. Am. Chem. Soc.* **2019**, *141*, 16243−16248.
(34) Yoval-Sánchez, B.; Rodríguez-Zavala, J. S. Differences in susceptibility to inactivation of human aldehyde dehydrogenases by lipid peroxidation byproducts. *Chem. Res. Toxicol.* **2012**, *25*, 722−729.
(35) Chen, C.-H.; Cruz, L. A.; Mochly-Rosen, D. Pharmacological recruitment of aldehyde dehydrogenase 3A1 (ALDH3A1) to assist ALDH2 in acetaldehyde and ethanol metabolism in vivo. *Proc. Natl. Acad. Sci. U. S. A.* **2015**, *112*, 3074−3079.
(36) Zhou, L.; Sheng, D.; Wang, D.; Ma, W.; Deng, Q.; Deng, L.; Liu, S. Identification of cancer-type specific expression patterns for

https://doi.org/10.1021/jacsau.4c00642
JACS Au 2024, 4, 3657−3667

active aldehyde dehydrogenase (ALDH) isoforms in ALDEFLUOR assay. *Cell Biol. Toxicol.* **2019**, *35*, 161−177.
(37) Moreb, J. S.; Muhoczy, D.; Ostmark, B.; Zucali, J. R. RNAi-mediated knockdown of aldehyde dehydrogenase class-1A1 and class-3A1 is specific and reveals that each contributes equally to the resistance against 4-hydroperoxycyclophosphamide. *Cancer Chemother. Pharmacol.* **2007**, *59*, 127−136.
(38) Li, M.; Xiong, T.; Du, J.; Tian, R.; Xiao, M.; Guo, L.; Long, S.; Fan, J.; Sun, W.; Shao, K.; et al. Superoxide radical photogenerator with amplification effect: Surmounting the Achilles' Heels of photodynamic oncotherapy. *J. Am. Chem. Soc.* **2019**, *141*, 2695−2702.
(39) Yu, L.; Xu, Y.; Pu, Z.; Kang, H.; Li, M.; Sessler, J. L.; Kim, J. S. Photocatalytic superoxide radical generator that induces pyroptosis in cancer cells. *J. Am. Chem. Soc.* **2022**, *144*, 11326−11337.
(40) Xu, Y.; Xiong, H.; Zhang, B.; Lee, I.; Xie, J.; Li, M.; Zhang, H.; Kim, J. S. Photodynamic Alzheimer's disease therapy: From molecular catalysis to photo-nanomedicine. *Coordin Chem. Rev.* **2022**, *470*, 214726.
(41) Tong, H.; Zhan, X.; Tian, X.; Li, J.; Qian, D.; Wu, D. Understanding the energy level matching relationships between semiconductor photocatalysts and organic pollutants for effective photocatalytic degradations. *J. Colloid Interface Sci.* **2018**, *526*, 384−391.
(42) Zhou, H.-M.; Zhang, J.-G.; Zhang, X.; Li, Q. Targeting cancer stem cells for reversing therapy resistance: Mechanism, signaling, and prospective agents. *Signal Transduct. Target. Ther.* **2021**, *6*, 62.
(43) Kim, J. H.; Park, J. M.; Jung, E.; Lee, J.; Han, J.; Kim, Y.-J.; Kim, J. Y.; Seo, J. H.; Kim, J. S. A synchronized dual drug delivery molecule targeting cancer stem cells in tumor heterogeneity and metastasis. *Biomaterials* **2022**, *289*, 121781.
(44) Croker, A. K.; Goodale, D.; Chu, J.; Postenka, C.; Hedley, B. D.; Hess, D. A.; Allan, A. L. High aldehyde dehydrogenase and expression of cancer stem cell markers selects for breast cancer cells with enhanced malignant and metastatic ability. *J. Cell. Mol. Med.* **2009**, *13*, 2236−2252.
(45) Li, M.; Kim, J.; Rha, H.; Son, S.; Levine, M. S.; Xu, Y.; Sessler, J. L.; Kim, J. S. Photon-Controlled Pyroptosis Activation (PhotoPyro): An Emerging Trigger for Antitumor Immune Response. *J. Am. Chem. Soc.* **2023**, *145*, 6007−6023.
(46) Xu, Y.; Chau, C. V.; Lee, J.; Sedgwick, A. C.; Yu, L.; Li, M.; Peng, X.; Kim, J. S.; Sessler, J. L. Lutetium texaphyrin: A photocatalyst that triggers pyroptosis via biomolecular photoredox catalysis. *Proc. Natl. Acad. Sci. U. S. A.* **2024**, *121*, No. e2314620121.
(47) Zhang, Z.; Zhang, H.; Li, D.; Zhou, X.; Qin, Q.; Zhang, Q. Caspase-3-mediated GSDME induced Pyroptosis in breast cancer cells through the ROS/JNK signalling pathway. *J. Cell. Mol. Med.* **2021**, *25*, 8159−8168.
(48) Kayagaki, N.; Stowe, I. B.; Lee, B. L.; O'Rourke, K.; Anderson, K.; Warming, S.; Cuellar, T.; Haley, B.; Roose-Girma, M.; Phung, Q. T.; et al. Caspase-11 cleaves gasdermin D for non-canonical inflammasome signalling. *Nature* **2015**, *526*, 666−671.
(49) Szabo, C. Hydrogen sulfide, an endogenous stimulator of mitochondrial function in cancer cells. *Cells* **2021**, *10*, 220.
(50) Nedeljković, M.; Damjanović, A. Mechanisms of chemotherapy resistance in triple-negative breast cancer-how we can rise to the challenge. *Cells* **2019**, *8*, 957.
(51) He, L.; Wick, N.; Germans, S. K.; Peng, Y. The role of breast cancer stem cells in chemoresistance and metastasis in triple-negative breast cancer. *Cancers* **2021**, *13*, 6209.
(52) Vishnubalaji, R.; Manikandan, M.; Fahad, M.; Hamam, R.; Alfayez, M.; Kassem, M.; Aldahmash, A.; Alajez, N. M. Molecular profiling of ALDH1+ colorectal cancer stem cells reveals preferential activation of MAPK, FAK, and oxidative stress pro-survival signalling pathways. *Oncotarget* **2018**, *9*, 13551−13564.

https://doi.org/10.1021/jacsau.4c00642
JACS Au 2024, 4, 3657−3667